Modal Test and Analysis of the NASA Tiltrotor Test Rig

Carl R. Russell **C. W. Acree, Jr.**

Aeromechanics Office
NASA Ames Research Center
Moffett Field, CA

The Tiltrotor Test Rig (TTR) is being developed at the NASA Ames Research Center for testing full-scale proprotors in the National Full-scale Aerodynamics Complex (NFAC) wind tunnel. The TTR is currently undergoing checkout testing to ensure its proper functionality. Part of the checkout process is a ground vibration test, or shake test, to characterize the modal characteristics of the test rig once it is installed in the wind tunnel. This paper presents a summary of the shake test procedure and an overview of the test results. The results include frequency response functions for a number of different test configurations as well as visualizations of the major mode shapes. Excitation methods included random and swept sine shaking as well as hammer impacts. At the conclusion of this paper, some recommendations are given for future shake tests.

NOMENCLATURE

FRF	Frequency Response Function
LRTA	Large Rotor Test Apparatus
MAC	Modal Assurance Criterion
MIMO	Multiple Input Multiple Output
NFAC	National Full-scale Aerodynamics Complex
RTA	Rotor Test Apparatus
TTR	Tiltrotor Test Rig

INTRODUCTION

The Tiltrotor Test Rig (TTR), which represents a new and unique experimental capability at NASA Ames Research Center, was recently installed in the 40- by 80-ft test section of the National Full-Scale Aerodynamics Complex (NFAC). The TTR is a NASA project, joint with the Army and Air Force, to develop a new, large-scale proprotor test system. It is designed to test advanced proprotors up to 26 feet in diameter at speeds up to 300 knots in airplane mode and up to 120 knots in helicopter mode.

The TTR is designed for use in both the 40- by 80- and 80- by 120-foot test sections of the NFAC. Unlike the Rotor Test Apparatus (RTA) and Large Rotor Test Apparatus (LRTA), the TTR is a horizontal axis rig and rotates on the test-section turntable to face the rotor into the wind in airplane mode, or fly edgewise at low speed in helicopter mode, or at any angle in between (Fig 1). Prior to operating the TTR in the wind tunnel, it is necessary to understand the dynamic characteristics of the test stand, particularly as they relate to whirl flutter and other potential instabilities. In addition, the TTR has a dedicated rotor balance, whose modal response must be known in order to accurately measure rotor loads.

Presented at the AHS International Technical Conference on Aeromechanics Design for Transformative Vertical Flight, San Francisco, CA, Jan 16-18, 2018.

For the first wind tunnel test, the TTR uses a research rotor derived from the right-hand rotor of the AW 609; herein, this research rotor is referred to simply as "609". Any similar proprotor can potentially experience dynamic instability, even when mounted on a test rig. In order to ensure adequate stability at high speeds, the dynamic behavior of the TTR must be thoroughly understood. Stability analyses of the TTR/609 are reported separately in Ref. 1.

The TTR weighs 60,000 lb and is mounted on 16-ft high struts (Fig 1). The large mass can dynamically couple with the turntable structure, and the high vertical moment arm can create enough bending in the struts to significantly modify the modal response. Experience with the RTA and LRTA showed that NASTRAN analyses alone were inadequate to properly characterize the modal behavior of those rigs [Refs. 2 and 3].

Building on experience gained from modal testing of other large-scale rotor test rigs, including the RTA and LRTA, an extensive ground vibration test was performed on the TTR. The results of this test were used to determine the mode shapes of the test stand as well as the associated frequency and damping values. This paper describes the modal test setup and procedure, gives an overview of results, shows comparisons with finite-element model results, and provides recommendations for future modal testing and analysis of rotor test stands.

METHODOLOGY

This section describes the methodology used to perform the shake test, followed by a description of the modal analysis.

Modal Test Setup

The primary method of the modal test was a large-scale shake test. Impact testing was also performed to compare with the shake test results. The shake test setup is shown in Figs. 2-7.

Excitation of the TTR was accomplished with a hydraulic shaker that was backstopped against a 12,000-lb reaction mass. The shaker had a bandwidth of 0 to 40 Hz, giving a maximum excitation frequency well above the maximum 3/rev frequency (28.45 Hz) of the 3-bladed 609 rotor. The input loads were measured with a 1000-lb capacity load cell. Random shaking was used to excite the TTR from 0 to 40 Hz at yaw angles of 0 deg (airplane mode) and 90 deg (helicopter mode). Once random shaking had identified modal frequencies, swept sine shaking over limited frequency bands was performed. The complete test matrix is given in Table 1.

The input loads were applied at three locations: the hub, the forward lifting lug, and the port aft lifting lug. The aft lifting lugs form a symmetric pair, so it was sufficient to apply loads at only one aft location. Most helicopters and large-scale rotor test stands, such as the RTA and LRTA, have very stiff output shafts. The TTR has a relatively flexible output shaft, so there was concern that not all of the modes could be sufficiently excited by shaking at the hub alone. The lifting lugs are much more rigidly attached to the TTR chassis, so excitation was performed at these two additional locations to ensure all modes were detected.

In general, the maximum peak-to-peak amplitude of the excitation was approximately ±800 lb. The only exception was a single data point of random shaking at 0 deg yaw in the lateral direction with an amplitude of approximately ±200 lb. This low-amplitude point was taken to look for evidence of non-linear damping in the system. The general strategy employed for this test was to introduce as much energy into the system as possible in order to get accurate damping measurements for the various modes; therefore, the vast majority of the shake test data were collected using high-amplitude input.

The swept sine runs were intended to increase the amount of energy injected into the system, particularly at the modal frequencies, in order to obtain accurate results. In practice, with the setup used for this test, it was very difficult to maintain proper alignment of the shaker for swept sine runs. Swept sine excitation was therefore not always effective at isolating and identifying all of the natural modes, particularly at low frequencies (below approximately 5 Hz).

Based on experience with the RTA and LRTA detailed in Refs. 2 and 3, which showed that hub mass has a significant impact on test stand frequency response, two different hub masses were tested here. A dummy hub, shown in Fig. 7, was installed on the TTR output shaft to serve two purposes. The first was to act as an attachment point for the shake test hardware. The second was to simulate the mass of the 609 rotor. The dummy hub includes removable mass blocks to adjust the hub weight. The shake test was carried out for all of the test conditions listed in Table 1 using both the 609 hub mass and the bare dummy hub with several of the mass blocks removed – a difference of 122 lb.

The response of the system was measured by the TTR rotor balance and by accelerometers installed at 21 different locations. The locations and directions of the accelerometers are shown in Fig. 8. For aeroelastic stability, the relative displacements of the hub, swashplate, and control actuators are important, in that order. On the TTR, the actuator mounting ring is bolted directly to the metric side of the balance, so a single set of accelerometers simultaneously measures the mode shapes of the actuators and the dynamic response at the balance. This accelerometer set is labeled "balance" in Fig. 8.

Additional accelerometer locations were necessary for accurate mode shape identification and to provide data for validating the NASTRAN model. Measurements were also taken for various on-board components, such as the drive motors and electronic cabinets. These items had only weak dynamic response and are not further discussed herein.

The data were collected with a 48-channel analyzer and processed to generate frequency response functions (FRFs) for each measurement. The balance gauge FRFs were combined and used to calculate amplification factors for the balance as a function of frequency. The accelerometer data were used to construct mode shapes and compute frequency and damping for each mode.

An impact test was also performed to determine whether it could produce the same results as the shake test. A 5-lb instrumented hammer was used, with a very soft rubber tip to ensure good low-frequency response. The response was measured by the same accelerometers and balance gauges as those used for the shake test. The excitation locations and configurations were the same as for the shake test, but with additional testing at a yaw angle of 45 deg.

Due to its complexity, the shake test requires a significant amount of time and planning to execute. A large amount of hardware is needed, including custom-made attachment fixtures, the facility bridge crane to support the reaction mass, and the hydraulic system required to operate the shaker. Additionally, the task of aligning the reaction mass, especially at multiple yaw angles, is time-consuming and makes a shake test of this scale take several weeks. The ability to perform an impact test in lieu of the shake test is highly desirable, as it would greatly reduce the amount of time required for modal testing.

Modal Analysis

Mode shapes were extracted from the accelerometer data using the ME'scope modal analysis software [Ref. 4]. The curve fitting functions of the software were used to determine

frequency and damping of the various mode shapes. One challenge with using ME'scope is that it does not provide the ability to quantify the quality of any given curve fit other than to inspect it visually. A "good fit" was therefore up to the judgement of the user. This may have an effect on the accuracy of the results, particularly with respect to damping. These effects are discussed in the Results section.

The ME'scope software provides the ability make mode shape calculations based on multiple-input-multiple-output (MIMO) data; however, for the data collected during this test, single-input calculations produced better results. This means that for all of the modal information presented in the Results section, modes dominated by, for example, vertical motion, are acquired only from vertical excitation. Similarly, lateral mode data comes only from lateral shaking, and longitudinal mode data comes only from longitudinal excitation.

As outlined in the previous section, results were obtained for several different configurations and excitation types. The frequency and damping values were extracted separately for each of the shake configurations for comparison between methods. The extracted mode shapes and associated frequency and damping values were then used for dynamic stability analysis. The results and methodology of the stability analysis are discussed in Ref 1.

RESULTS

The results are organized as follows. First, magnitude and phase plots for the hub accelerometer and rotor balance response are presented, along with identification of the observed mode shapes and comparison with NASTRAN results. Next, the effect of excitation type is examined, with results shown for random and swept sine shaking, and impact testing. Results at different yaw angles follow, showing the differences between the results in airplane, conversion, and helicopter modes. The effect of hub mass is presented, followed by a brief discussion of damping calculation accuracy.

Mode Identification

Figures 9-11 show frequency response functions (FRFs) for random shaking at the hub. Magnitude and phase are plotted for the hub accelerometer in the direction of excitation. Figures 12-14 show the FRFs measured at the TTR balance. Six modes can be identified by inspection of the FRF plots. Vertical modes are seen at 8.4, 11.4, and 17.1 Hz. There are two obvious lateral modes at 2.0 Hz and 14.8 Hz, and one clear longitudinal mode at 2.6 Hz. Fig. 11 shows two additional peaks at 11.4 and 14.8 Hz, which are two of the primarily in-plane modes that have minor longitudinal components. Using the modal analysis software with the complete set of accelerometer data, two additional modes were identified: a lateral mode at 2.6 Hz and a vertical mode at 15.3 Hz. All of these modes, identified as Modes 1-8, along with their shape descriptions and damping values are given in Table 2 and identified in Figs. 9-14.

Part of the challenge with identifying Mode 3, the yaw mode about the forward strut, is that it has an almost identical natural frequency to that of Mode 2, the longitudinal strut mode. Mode 2 is very lightly damped, so even a slight misalignment of the shaker in the lateral shake configuration can cause the longitudinal mode to become excited, extracting energy from the system and making the more heavily damped Mode 3 difficult to identify. Shaker alignment was particularly problematic for swept sine shaking, as discussed in the Methodology section. As will be shown in a later section, this issue can be mitigated by lowering the shake amplitude or using an impact test instead.

The balance results in Figs. 12-14 show similar results to the hub accelerometer FRFs, but with opposite phase angle. The maximum amplification factors at the balance are quite high, especially for the in-plane directions. The 11.4-Hz vertical mode causes an amplification of 55 times the input load, while the 14.8-Hz lateral mode causes an amplification factor of 44. While not necessarily problematic, it will be important for TTR operations to avoid 1/rev and N/rev frequencies near these modes. For the 3-bladed 609 rotor, the primary operational speeds are 478 rpm in airplane mode and 569 rpm in hover mode. These rotor speeds correspond to 1/rev frequencies of 7.97 Hz and 9.48 Hz. The 3/rev frequencies of the 609 rotor are 23.90 Hz and 28.45 Hz, so its testing will avoid the highest peaks in the frequency response.

Figures 15 and 16 show a comparison between two of the experimentally determined mode shapes and the corresponding mode shapes determined by NASTRAN. For clarity, several of the accelerometer nodes are omitted from Figs. 15 and 16. The dotted lines in the lower images show the un-deflected accelerometer locations, with the solid lines showing the deflected shape. The mode shapes are generally in good agreement between analysis and test, but there is significant error in most of the predicted frequencies. Table 2 includes the frequencies that were predicted by NASTRAN for each of the 8 identified modes, and Fig. 17 shows a visual comparison of the frequencies obtained by experiment and analysis. On average, NASTRAN over-predicts the modal frequencies by 24%. The cause of the NASTRAN errors is believed to be known and is undergoing investigation.

For whirl flutter stability analysis, the most important modes to properly identify are the low-frequency modes – Modes 1-3 in Table 2. In particular, the stability analysis requires the relative modal displacements of the hub, swashplate, and actuators (measured at the balance). As a check on the accuracy of the experimental data, the mode shapes measured at these three locations were compared with NASTRAN results using the Modal Assurance Criterion (MAC) [Ref. 5].

For two normal mode shapes represented by vectors φ_1 and φ_2, the equation for MAC is given by:

$$MAC(\varphi_1, \varphi_2) = \frac{\varphi_1^t \varphi_2}{(\varphi_1^t \varphi_1)(\varphi_2^t \varphi_2)}$$

MAC takes on values between 0 and 1, with a value of 0 indicating two mode shapes are completely uncorrelated and a value of 1 indicating perfect correlation. For modes 1, 2, and 3, the MAC values between the NASTRAN model and random shake test results are 0.998, 0.994, and 0.937, respectively, indicating very good correlation between the test and analysis for these mode shapes. MAC does not include frequency or damping values, and even though the mode shapes are well matched between analysis and test, the frequency and damping values are not.

Excitation Types

This section gives a comparison of results using different excitation techniques. All of the results presented in the following sections are for excitation at the hub. As discussed in the Methodology section, shaking and impact testing were also performed at two lifting lugs in order to ensure excitation of all modes. The results showed that hub excitation was indeed sufficient to detect all of the TTR modes over the frequency range of interest. Lifting lug excitation results were very similar to (and in some cases actually of worse quality than) those obtained for hub excitation and are therefore largely omitted from this paper. Table 3 summarizes the modal frequency and damping results for the various excitation types, locations, and directions. As noted in the table, not all excitation methods were effective at identifying every mode.

Figures 18-20 show the magnitude of the hub accelerometer response to random and swept sine shaking as well as to a hammer impact. Figures 21-23 are re-scaled versions of these results showing only the low-frequency response. To investigate the effect of input magnitude, a single random shake run at low amplitude (approximately ±200 lb) was performed in the lateral direction at the hub. For all other excitation directions and locations, including random and swept sine, the maximum input amplitude was approximately ±800 lb.

For the vertical excitation results shown in Fig. 18, there are only minor differences between the different excitation methods near the peaks. Off-peak, there are significant differences between the methods, particularly at low frequencies. The swept sine response is much smoother than the random shaking response below 5 Hz, but there are no vertical modes in this frequency range, so a smooth response is not particularly important there. The random and swept sine shake tests result in slightly lower natural frequencies than the impact tests, which indicates non-linearities in damping. The frequency and damping results obtained with the ME'scope curve fitting software for all of the excitation methods are given in Table 3.

For the lateral excitation results, shown in Fig. 19, the differences between methods are more pronounced. In particular, the second lateral strut mode, at 2.59 Hz, is barely visible in the results for high-amplitude random shaking and very weak for swept sine excitation (and at a significantly higher frequency). When the input amplitude of the random shaking is reduced, the second lateral strut mode becomes clearly identifiable. In addition, the low amplitude random excitation results closely match the impact test results.

Finally, for the longitudinal excitation (Fig. 20), there is really only one peak of interest, at 2.58 Hz. The swept sine and random shake results are nearly identical, while the impact test results look quite different from the others. At the 2.58-Hz peak, however, the impact test results closely match the shake test results. As mentioned earlier, the longitudinal strut mode and second lateral strut mode have nearly identical natural frequencies. This likely led to the large discrepancies in the low frequency results for lateral excitation.

The low-frequency results in Fig. 22 show that for the lateral strut modes, the low-amplitude random shake results are very close to the impact test results above 1 Hz, while the high-amplitude random response more closely matches the similarly high-amplitude swept sine results. The longitudinal strut mode response shown in Fig. 23 is nearly identical for random and swept sine excitation. The impact test results shown in Fig. 23 appear different from the shake results due to the plot scaling, but they really only differ by approximately 0.1 Hz. The resulting differences in the curve-fit frequency and damping values can be seen in Table 3.

Figures 24-26 show FRFs for the response measured at the balance for the same test runs as above. Similar trends to the hub accelerometer results can be seen for all three excitation directions. The high-amplitude random and swept sine responses match each other very closely, while the impact test results closely match those of the low-amplitude random excitation. Based on the results for all of the different excitation methods a few conclusions can be drawn regarding modal testing of the TTR:

- Impact testing produces very similar results to shake testing, particularly when the shake test magnitude is low.
- Due to non-linear damping of the TTR structure, impact testing will generally result in slightly higher modal frequencies (on the order of 0.1 Hz) and variations in modal damping.
- For all excitation methods, there is good agreement between modal frequencies, with typical frequency

variations between methods of no more than 0.2 Hz, and a couple of outliers at 0.3 and 0.7 Hz.

It is very difficult to maintain proper alignment of the shaker for swept sine excitation so it is probably more effective to vary the amplitude of random shaking to identify structural non-linearities

Yaw Angle

Yaw angle as used here refers to the angle of the turntable. For the purposes of this work, 0 deg refers to airplane mode, with the TTR aligned with the flow. 90 deg refers to helicopter mode, with the TTR perpendicular to the flow. Figs. 1-3 show the different yaw angles tested. The highest-airspeed testing will occur in airplane mode, so it was most important to obtain good results at 0 deg yaw; therefore, more time was devoted to testing at 0 deg. Two different yaw angles were tested with shaker excitation and three yaw angles were tested with impact excitation. The effects of yaw angle on the response of the hub accelerometer are shown in Figs. 27-32. Figures 27-29 show the results using random excitation, while Figs. 30-32 show the results for impact excitation. In general, the differences in modal characteristics between TTR yaw angles are minor. The resulting tabulated frequencies and damping are included in Table 3.

The most noticeable difference between results at the different yaw angles are for the two higher frequency vertical modes at approximately 15 and 17 Hz (Modes 7 and 8). In both the shake test (random and swept sine) and impact test results, Mode 8 could not be fit by the modal analysis software. This does not necessarily mean that the mode disappeared; only that it was not excited with enough energy to distinguish it from Mode 7. Mode 7, meanwhile, dropped in frequency as yaw was increased to 90 deg, with a change of approximately 1 Hz. For the two lower frequency vertical modes as well as all of the lateral and longitudinal modes, the response remains largely unchanged with different yaw angles.

Hub Mass

Finally, two different hub masses were tested. All of the results shown thus far have used the complete 609 dummy hub shown in Fig. 7. An additional set of runs at all of the conditions listed in Table 1 was performed with most of the mass blocks on the dummy hub removed. A single mass block was left installed because the shaker needed to attach to the mass block for in-plane shaking. The total removed weight was 122 lb.

Figures 33-35 show the effect of removing the mass blocks. The results shown here are for random excitation, but similar trends were observed for the other excitation methods. Based on previous experience with vibration testing of the RTA and LRTA [Refs. 2 and 3], the expectation was that hub mass would have a significant impact on the frequency response, particularly for modes primarily involving motion of the hub. As expected, lowering the hub mass by 122 lb had no effect on the low-frequency strut modes, but it increased the frequencies of the higher-frequency shaft-bending modes. As the mass of the TTR is on the order of 60,000 lb, a change of 122 lb does not have a significant impact on the modal mass of the strut modes, which involve motion of the entire TTR. For the shaft bending modes that primarily involve hub motion, the modal mass is on the order of 1,000 lb, so 122 lb is a significant change that will impact modal frequency.

Damping accuracy

As shown in Table 3, damping values for different excitation methods can vary significantly in cases where variation would not normally be expected. Some of this variation may be attributed to non-linear damping in the structure, as previously discussed. In other cases, the source of the discrepancy is harder to explain. An example of such a discrepancy is the difference in damping for Mode 1 when shaking at the forward lifting lug (4.10% critical) vs. shaking at the aft lifting lug (1.17% critical).

In both cases, the shake application point is not at a node of the mode shape, and the attachment point of the shaker is rigidly connected to the TTR chassis, so similar results would be expected. As previously discussed, the modal analysis software did not provide a means to quantify the quality of the curve fits. Whether the discrepancies in damping are due to shortcomings in the curve fitting methods or another source is the subject of ongoing study.

Figures 36 and 37 show comparisons of the modal damping values obtained for all excitation types at the hub and at the two lifting lugs. There is not a discernable pattern between methods as to whether one method consistently disagrees with the others or is particularly high or low compared with the others. There is a noticeable difference in the spread of damping values for the different modes. Modes 2, 5, and 6 have very consistent damping values between methods, while the others are more scattered. For the stability analysis performed in Ref. 1, the analysis generally used the damping value obtained from random shaking, though impact test values were used for cases where random shake values were not available (e.g., at 45 deg yaw).

SUMMARY AND CONCLUSIONS

This paper has presented an overview of the modal test and analysis performed for the Tiltrotor Test Rig installed in the 40- by 80-ft test section of the National Full-scale Aerodynamics Complex. Multiple excitation methods were used, including random shaking, swept sine shaking, and hammer impact. Hub mass and yaw angle were varied to determine their effects on dynamic response of the TTR.

Extensive accelerometer measurements were collected to determine the mode shapes and associated frequency and damping values for this installation of the TTR. Frequency response data were also collected for the rotor balance to determine force amplification factors over a range from 0 to 40 Hz. Based on the testing and analysis completed, the following conclusions and recommendations can be made:

With respect to excitation type:

The impact tests showed mostly good agreement with the shake test results with evidence of non-linear damping (i.e., lower modal frequencies resulting from the shake test than from the impact test).

Comparison of low- and high-magnitude shaking supported a conclusion of non-linear damping, especially in the low-frequency strut modes.

Based on the results shown here, impact testing is an acceptable substitute for shake testing of the TTR for frequency identification; however, modal damping obtained from impact testing showed variations when compared with results from shake testing.

For the most part, swept sine excitation did not result in significantly different results from random excitation, except at low off-peak frequencies.

With respect to finite-element model comparison and modal characteristics:

Mode shapes showed good agreement between test and finite-element modeling; however, the frequencies were not well predicted by NASTRAN.

Excitation at the hub and two lifting lugs produced similar results, indicating that a single excitation point (the hub) is sufficient.

Attempting to curve fit results from multiple separately executed excitation locations and directions (MIMO analysis) did not produce acceptable results. Given the equipment available for this test, single input, multiple output analysis is necessary. It is possible that simultaneous excitation at multiple locations and/or directions would produce better results, but this was not tested.

With respect to TTR configuration:

Variations in hub mass had little to no impact on strut mode frequency or damping, but did have a significant impact on modes primarily involving motion of the hub (i.e., those between 10 and 20 Hz). Accurate hub mass during modal testing is therefore necessary to obtain an accurate frequency response of the TTR.

Different yaw angles of the TTR resulted in only minor differences in the frequency response.

Finally, some recommendations can be made for how the modal test results should be used for stability analysis. Of the methods tested, random shaking and impact testing at the hub produced the most reliable results in terms of consistently identifying the various modes. Furthermore, both of these methods show good agreement with each other in predicted frequencies and mode shapes for all hub masses and yaw angles tested. The mode shapes, in turn, match well with NASTRAN analysis as measured by the Modal Assurance Criterion.

The remaining difficulty is properly identifying modal damping. The damping values produced by impact testing appear reasonable, but show non-negligible differences from corresponding shake test values. For stability analysis, it is likely wise to consider results from both random excitation and impact testing, especially if marginal stability is found. Given the relative ease of impact testing over shake testing, it is desirable for future modal tests of large rotor test rigs, such as the TTR, to rely primarily on impact testing.

With respect to future TTR modal tests, if a major configuration change is made, such as a different rotor system or structural modifications, impact test results should be confirmed with a random shake test in at least one test rig orientation and hub mass. The effects of varying hub mass and yaw angle can then probably be measured by impact testing alone. Further investigation will be required to improve confidence in damping measurements before shake testing can be eliminated altogether.

ACKNOWLEDGEMENTS

The authors would like to acknowledge the contributions of the entire NFAC team of technicians and mechanics who ensured that this test was a success. In addition, the assistance of Farid Haddad, Frank Pichay, Alex Sheikman, Billy Bartow, Chris Hartley, and Tom Norman were invaluable. Xin Xin Nee provided the NASTRAN analysis, and TTR photographs were provided by Eduardo Solis.

REFERENCES

1. Kottapalli, S. and Acree Jr., C. W., “Analytical Performance, Loads, and Aeroelastic Stability of a Full-Scale Isolated Proprotor,” AHS Technical Meeting on Aeromechanics Design for Transformative Vertical Flight, San Francisco, CA, Jan 16-18, 2017.

2. Peterson, R. and van Aken, J., “Dynamic Calibration of the NASA Ames Rotor Test Apparatus Steady/Dynamic Rotor Balance,” NASA-TM-110393, April 1996.

3. Russell, C., "Shake Test Results and Dynamic Characterization of the Large Rotor Test Apparatus in the NFAC 40- by 80-Foot Wind Tunnel," NASA/TM-2015-218877, September 2015.

4. *ME'scopeVES – Overview*, Vibrant Technology, Inc., https://www.vibetech.com/mescope/mescopeves-overview/, accessed July 13, 2017.

5. Allemang, R. and Brown, D., "A Correlation Coefficient for Modal Vector Analysis," Proceedings of the 1st International Modal Analysis Conference (IMAC I), Orlando, FL, November 1982.

Figure 1. Tiltrotor Test Rig (TTR) installed with the 609 rotor in the 40- by 80-ft test section of the National Full-scale Aerodynamics Complex – 45 deg yaw (conversion mode)

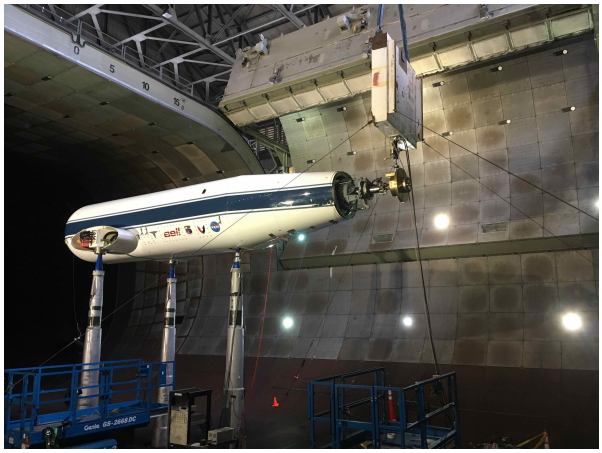

Figure 2. Shake test setup – vertical shaking at the hub – 0 deg yaw (airplane mode)

Figure 3. Shake test setup – lateral shaking at hub – 90 deg yaw (helicopter mode)

Figure 4. Shake test setup – longitudinal shaking at hub – 0 deg yaw (airplane mode)

Figure 5. Shake test setup – lateral shaking at forward lifting lug – 0 deg yaw (airplane mode)

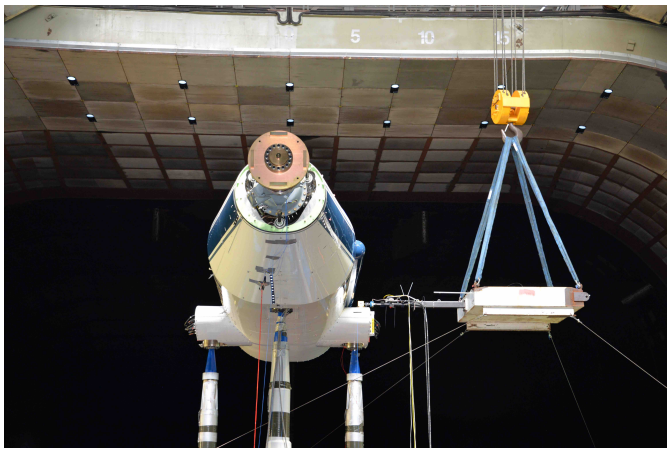

Figure 6. Shake test setup – lateral shaking at aft lifting lug – 0 deg yaw (airplane mode)

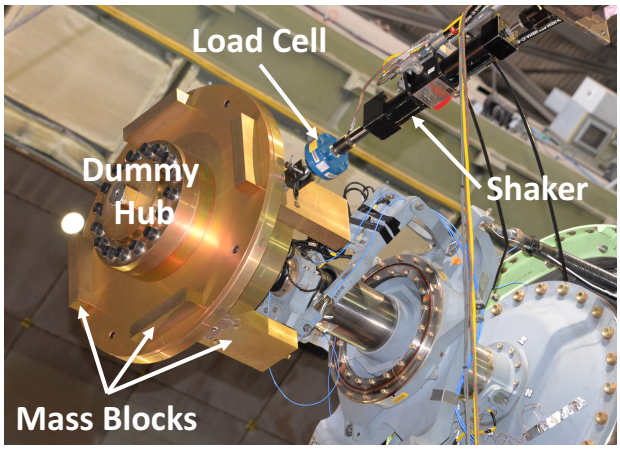

Figure 7. Shake test setup – hardware close-up – lateral shaking at hub

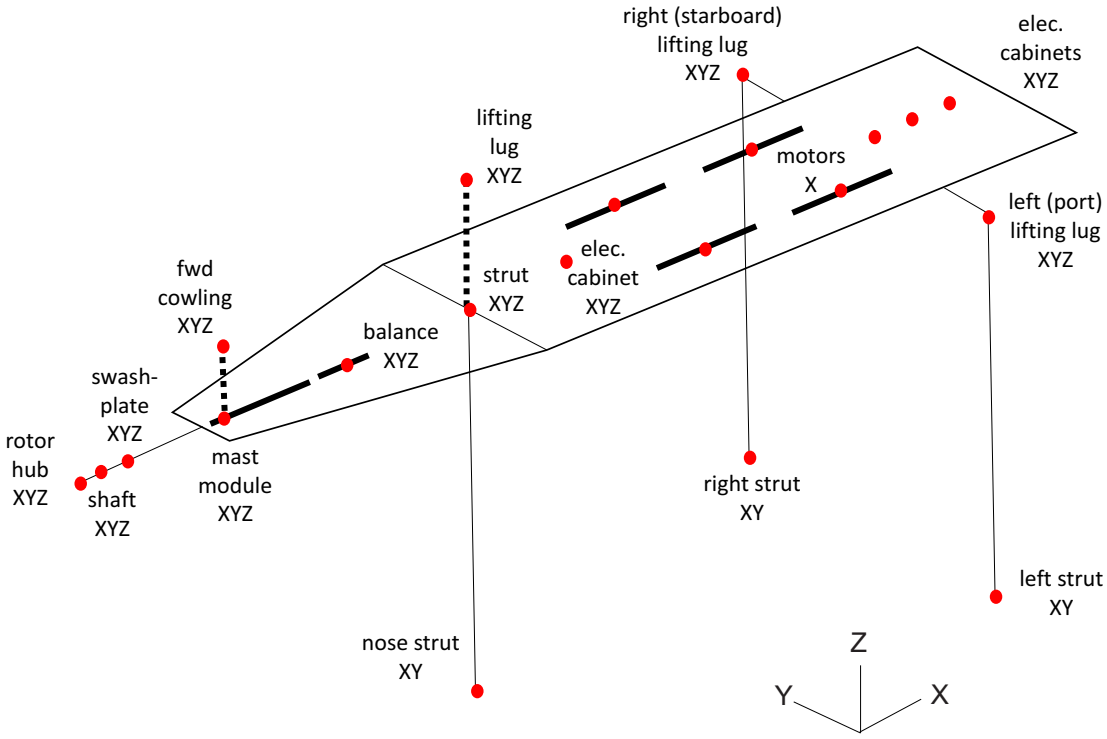

Figure 8. Accelerometer locations for the TTR shake test

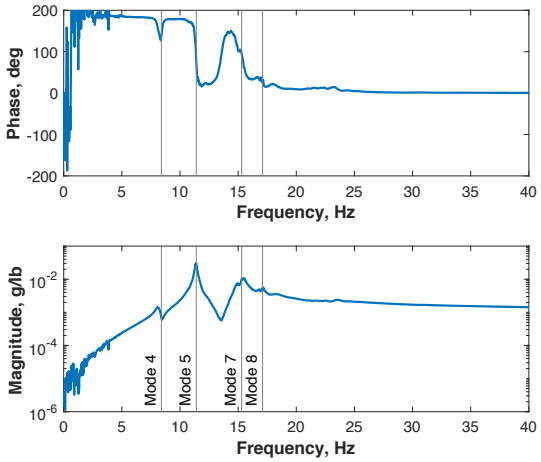

Figure 9. Hub accelerometer vertical response to vertical excitation

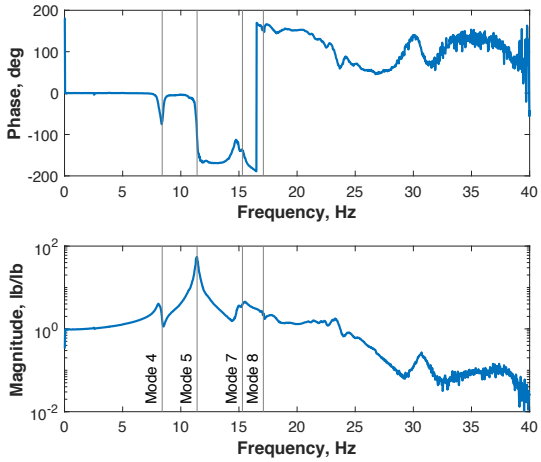

Figure 12. Balance vertical (side force gauge) response to vertical shaking

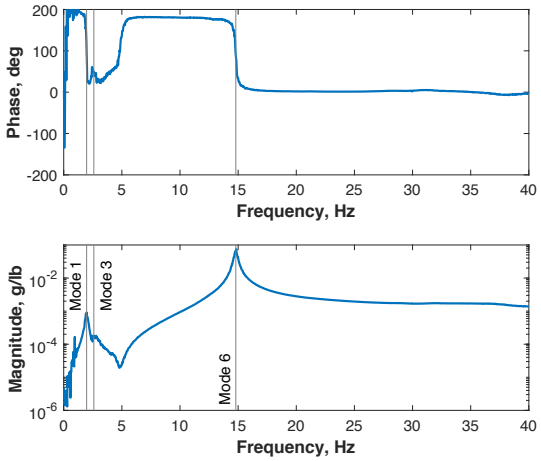

Figure 10. Hub accelerometer lateral response to lateral excitation

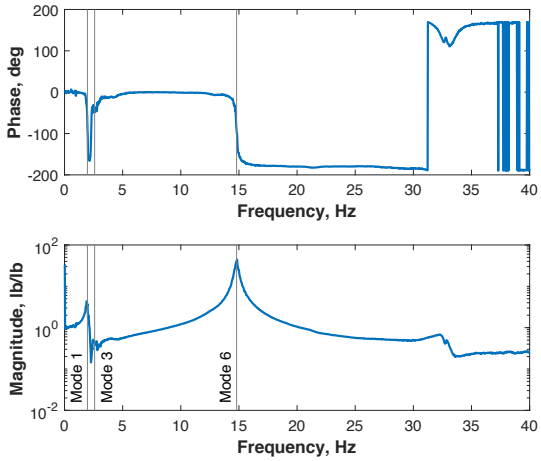

Figure 13. Balance lateral (axial force gauge) response to lateral shaking

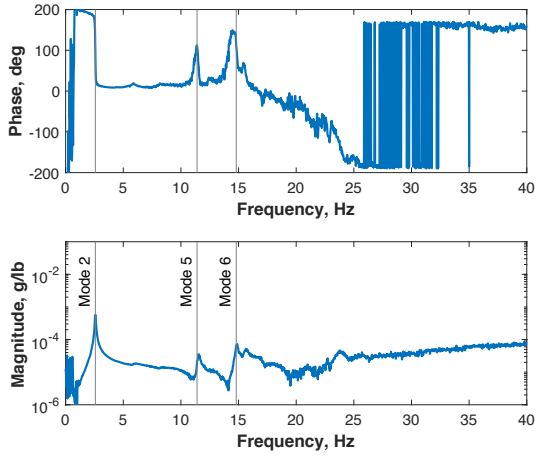

Figure 11. Hub accelerometer longitudinal response to longitudinal excitation

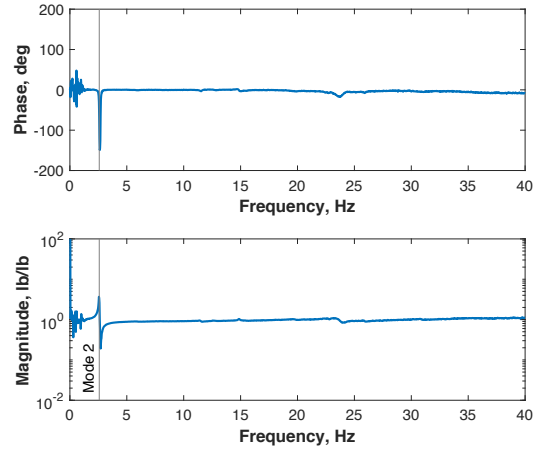

Figure 14. Balance longitudinal (normal force gauge) response to longitudinal shaking

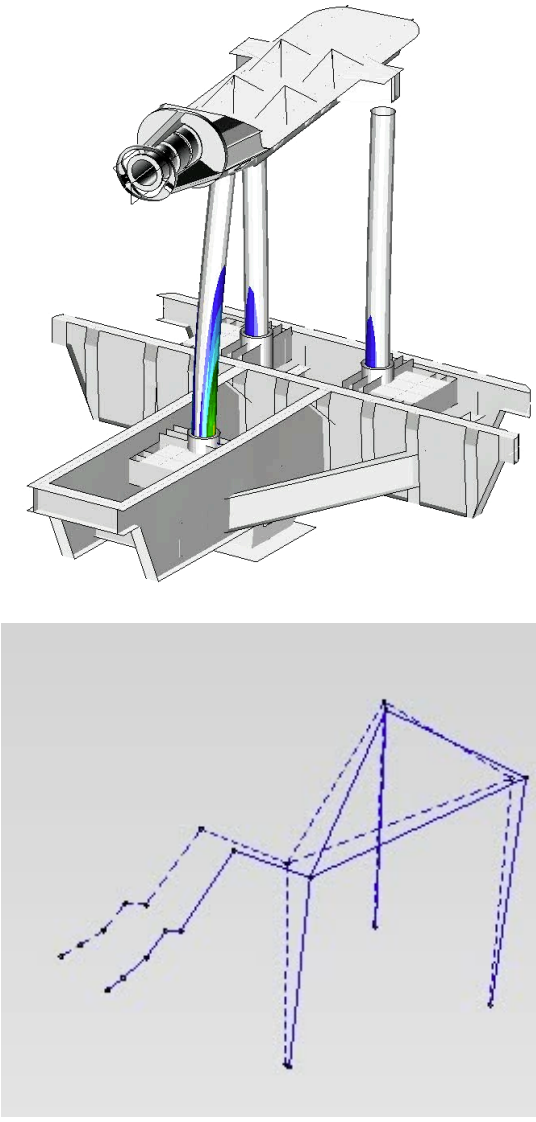

Figure 15. NASTRAN (top) and shake test (bottom) mode shape visualization for Mode 1

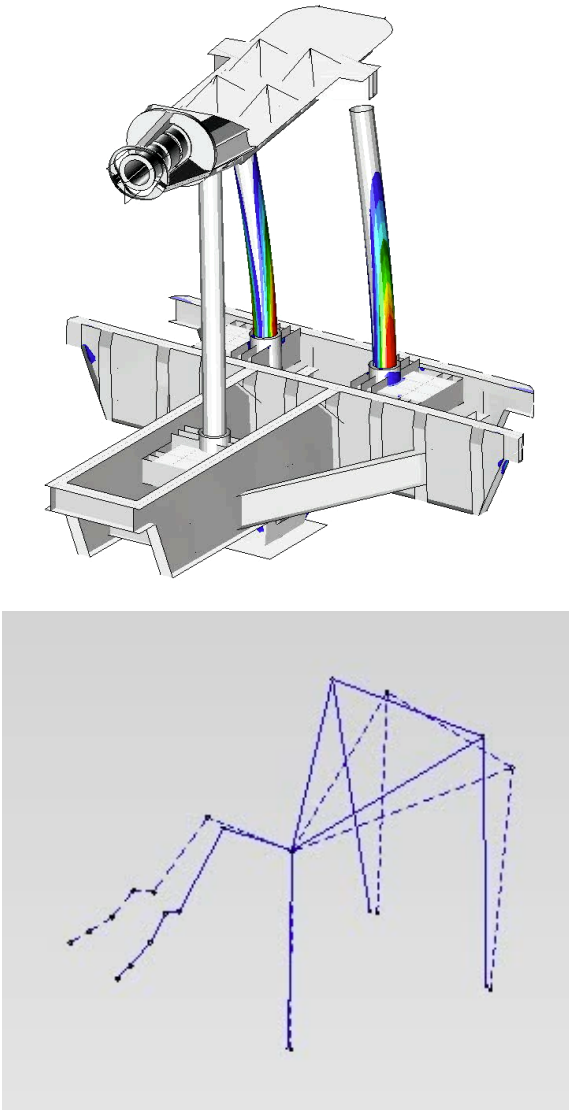

Figure 16. NASTRAN (top) and shake test (bottom) mode shape visualization for Mode 3

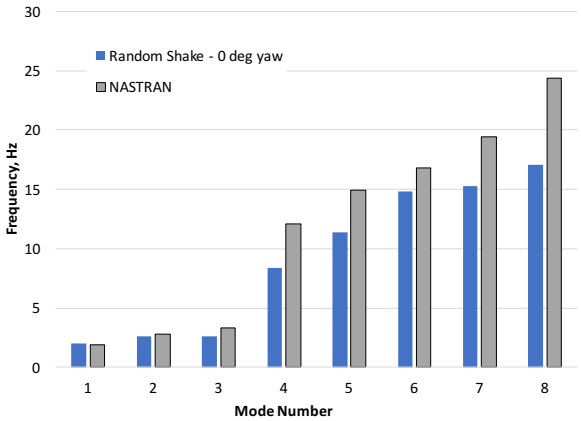

Figure 17. Comparison of NASTRAN and experimental modal frequencies

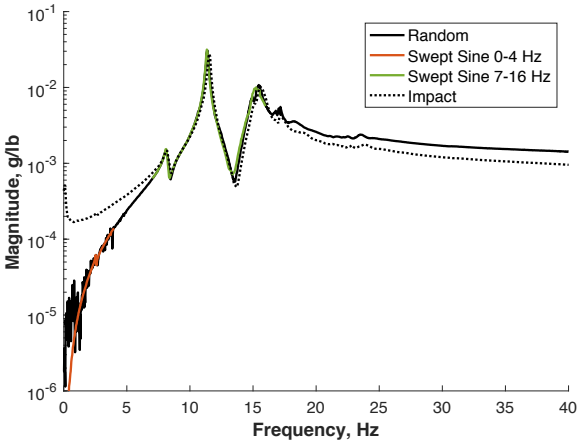

Figure 18. Vertical hub accelerometer response for various excitation methods

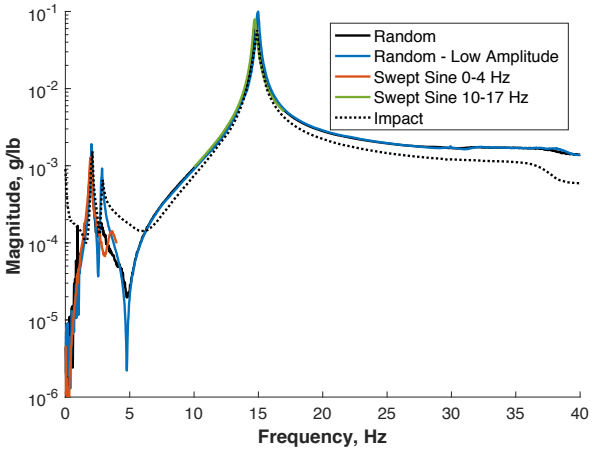

Figure 19. Lateral hub accelerometer response for various excitation methods

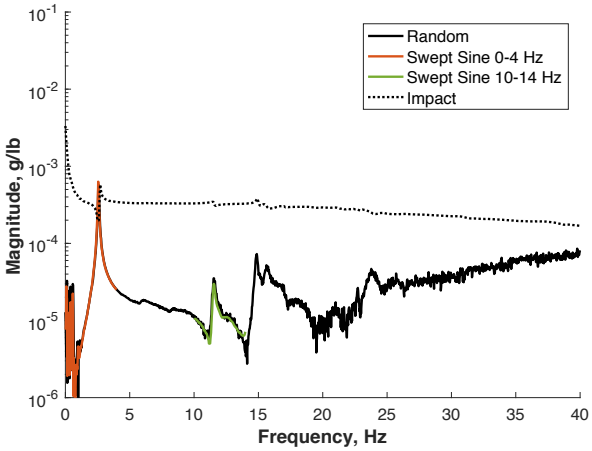

Figure 20. Longitudinal hub accelerometer response for various excitation methods

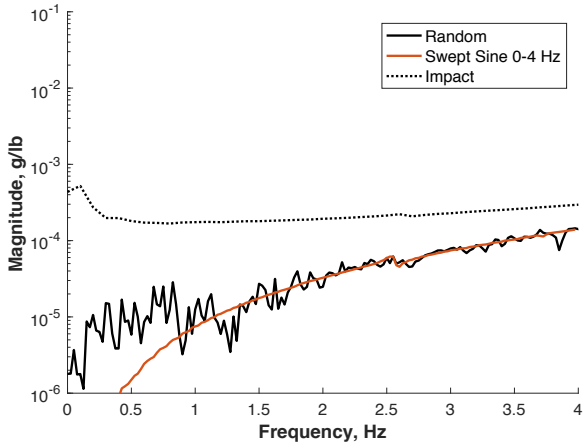

Figure 21. Low-frequency vertical hub accelerometer response for various excitation methods

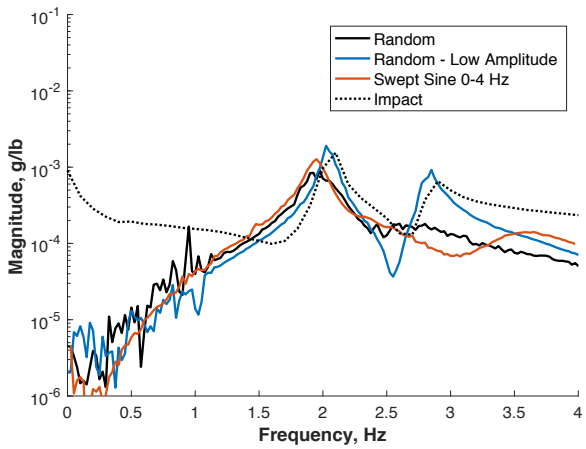

Figure 22. Low-frequency lateral hub accelerometer response for various excitation methods

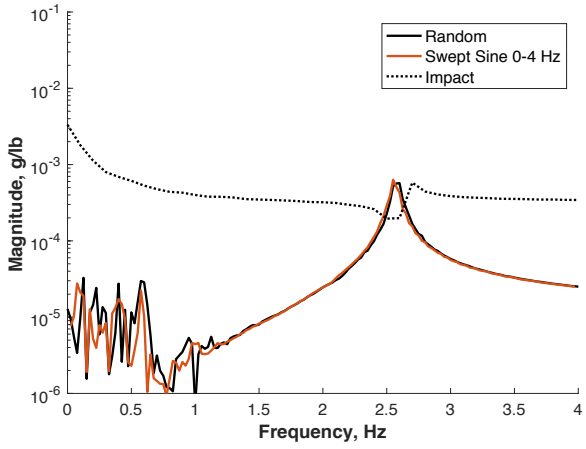

Figure 23. Low-frequency longitudinal hub accelerometer response for various excitation methods

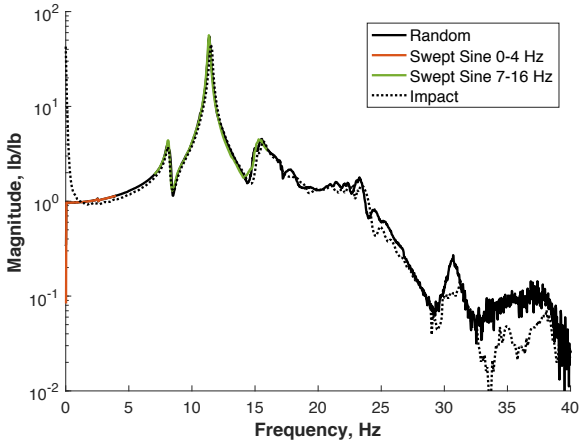

Figure 24. Vertical balance response for various excitation methods

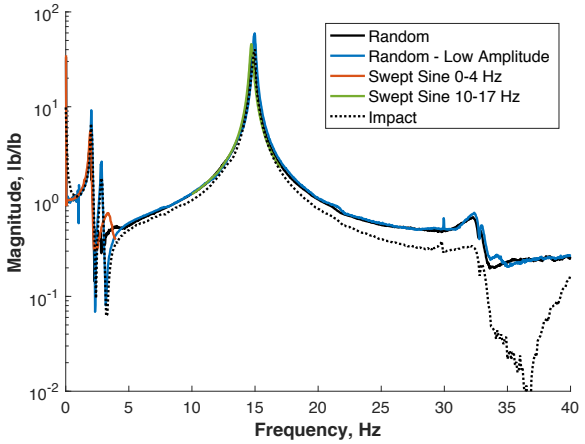

Figure 25. Lateral balance response for various excitation methods

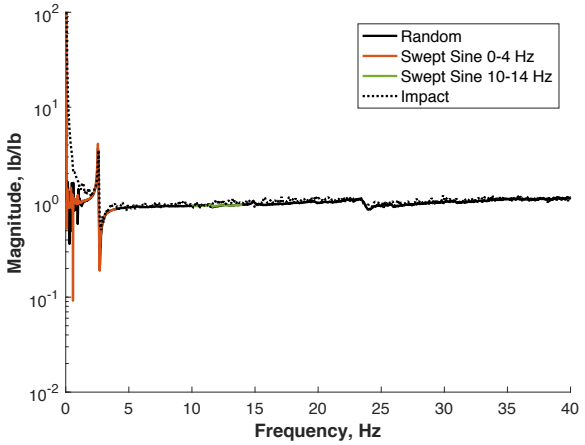

Figure 26. Longitudinal balance response for various excitation methods

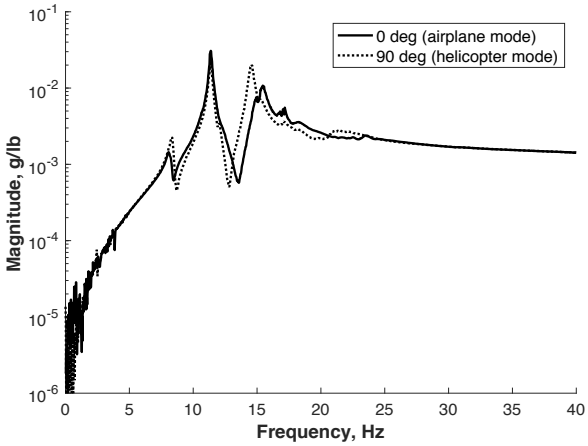

Figure 27. Effect of yaw angle on vertical hub response to random shaking

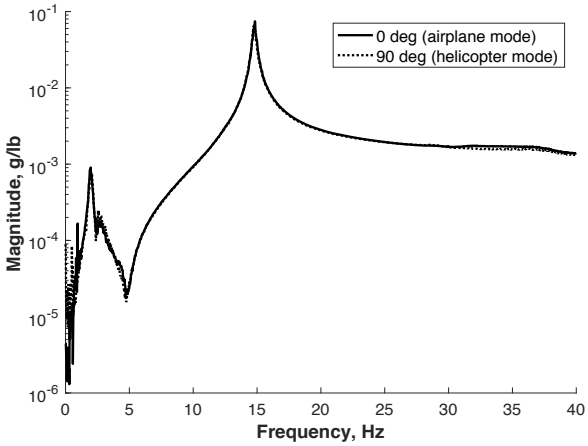

Figure 28. Effect of yaw angle on lateral hub response to random shaking

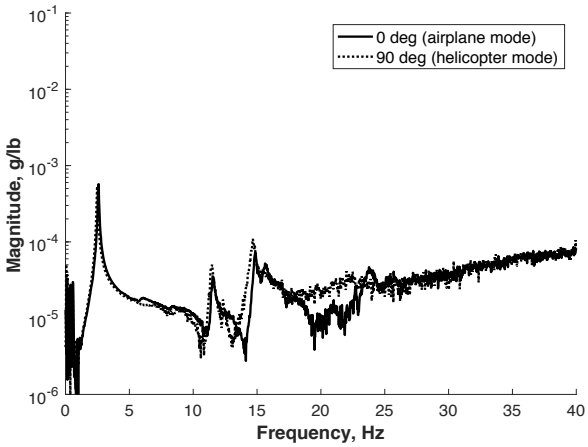

Figure 29. Effect of yaw angle on longitudinal hub response to random shaking

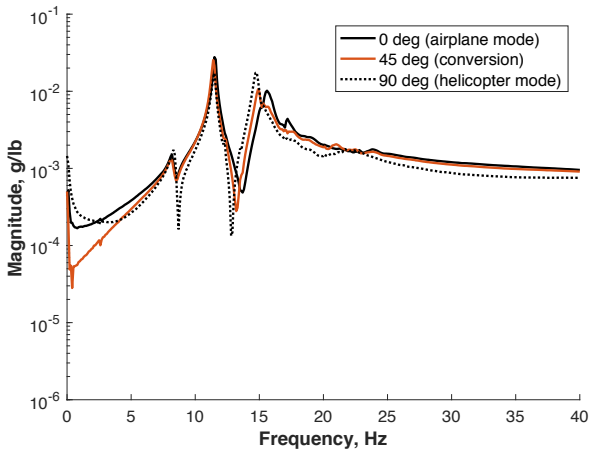

Figure 30. Effect of yaw angle on vertical hub response to impact

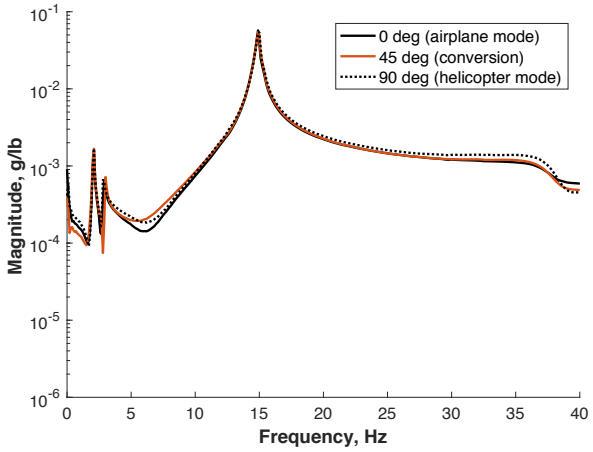

Figure 31. Effect of yaw angle on lateral hub response to impact

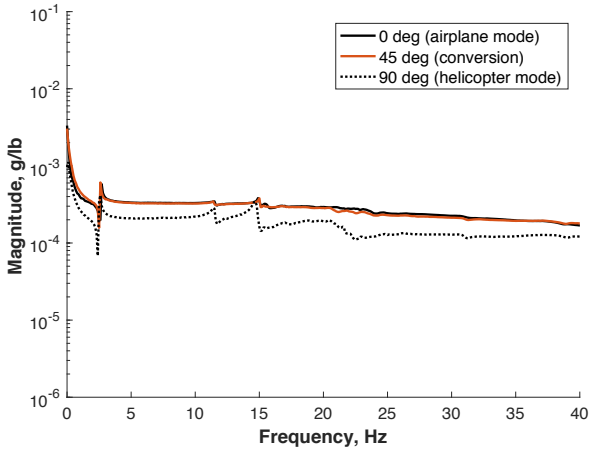

Figure 32. Effect of yaw angle on longitudinal hub response to impact

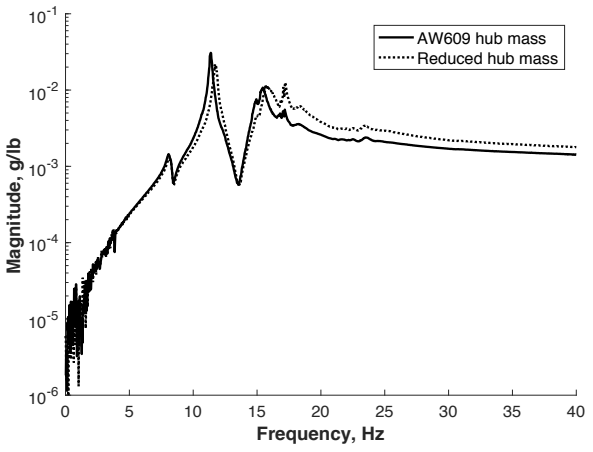

Figure 33. Effect of hub mass on vertical hub response to random shaking

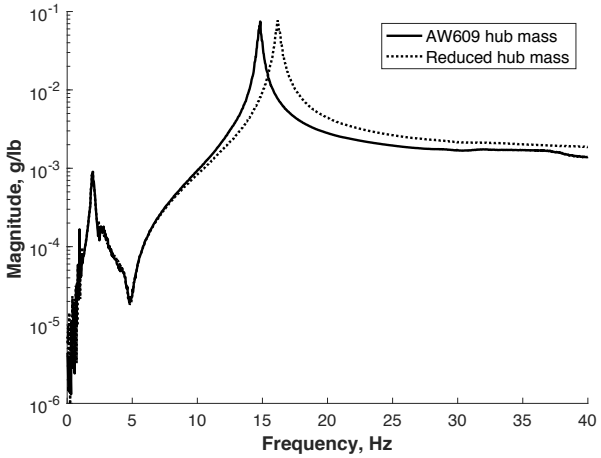

Figure 34. Effect of hub mass on lateral hub response to random shaking

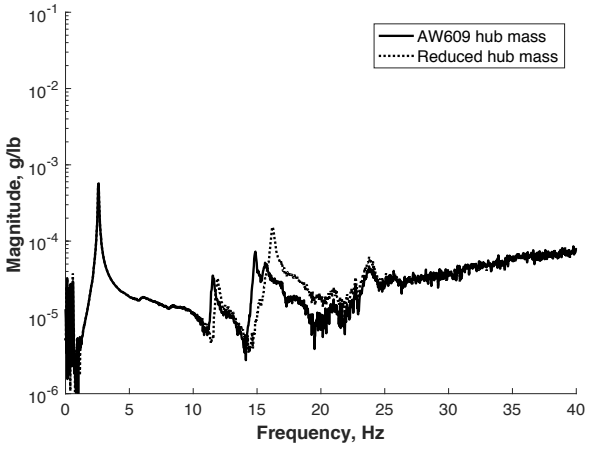

Figure 35. Effect of hub mass on longitudinal hub response to random shaking

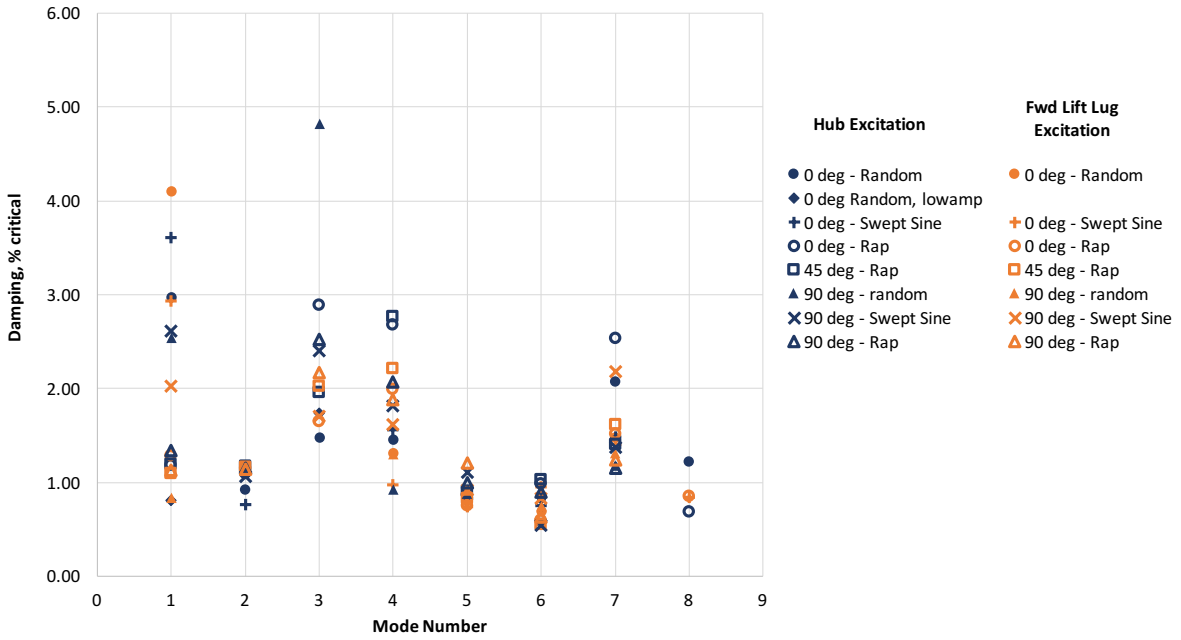

Figure 36. Comparison of modal damping values – hub and fwd lifting lug

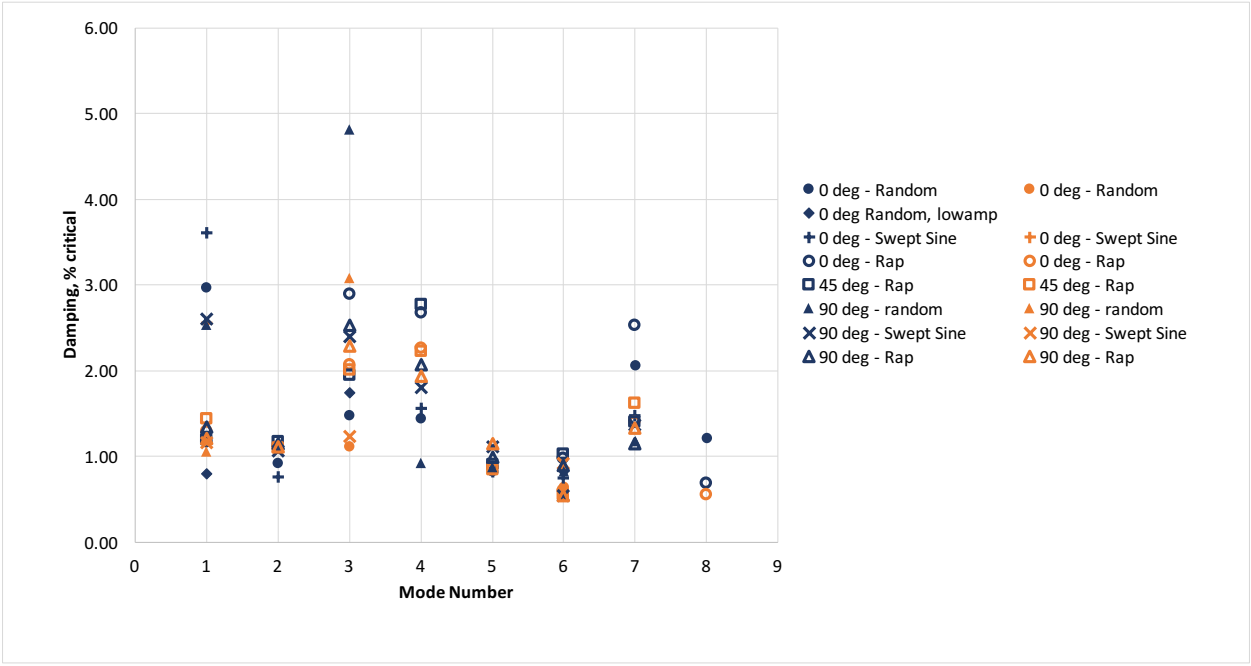

Figure 37. Comparison of modal damping values – hub and aft lifting lug

Table 1. TTR shake test matrix

Yaw	Excitation Location	Excitation Direction	Excitation Type
0	Hub	Vertical	Random, Swept Sine, Impact
		Lateral	Random, Random - Low Amplitude, Swept Sine, Impact
		Longitudinal	Random, Swept Sine, Impact
	Forward Lift Lug	Vertical	Random, Swept Sine, Impact
		Lateral	Random, Swept Sine, Impact
		Longitudinal	Impact
	Aft Port Lift Lug	Vertical	Impact
		Lateral	Random, Swept Sine, Impact
		Longitudinal	Impact
45	Hub	Vertical, Lateral, Longitudinal	Impact
	Forward Lift Lug	Vertical, Lateral, Longitudinal	Impact
	Aft Port Lift Lug	Vertical, Lateral, Longitudinal	Impact
90	Hub	Vertical	Random, Swept Sine, Impact
		Lateral	Random, Swept Sine, Impact
		Longitudinal	Random, Swept Sine, Impact
	Forward Lift Lug	Vertical	Random, Swept Sine, Impact
		Lateral	Random, Swept Sine, Impact
		Longitudinal	Impact
	Aft Port Lift Lug	Vertical	Impact
		Lateral	Random, Swept Sine, Impact
		Longitudinal	Impact

Table 2. Mode shape frequency and damping summary for random excitation at the hub

Mode No.	Frequency—Experiment, Hz	Frequency—NASTRAN, Hz	Damping—Experiment, % critical	Description
1	1.97	1.93	2.97	Yaw mode about aft struts
2	2.58	2.78	0.93	Longitudinal strut mode
3	2.59	3.32	1.48	Yaw mode about fwd strut
4	8.40	12.1	1.45	Vertical balance frame
5	11.4	14.9	0.83	TTR + balance frame pitch
6	14.8	16.8	0.84	Lateral shaft bending
7	15.3	19.4	2.07	Vertical shaft + TTR bending
8	17.1	24.4	1.22	TTR + vertical shaft bending

Table 3. Modal frequency and damping for all excitation methods

Hub Excitation

	Frequency, Hz								Damping, %							
	0 deg				45 deg	90 deg			0 deg				45 deg	90 deg		
Mode No	Random Shake	Random – low amp	Swept Sine	Impact	Impact	Random Shake	Swept Sine	Impact	Random Shake	Random – low amp	Swept Sine	Impact	Impact	Random Shake	Swept Sine	Impact
1	1.97	2.04	1.95	2.06	2.05	1.99	1.98	2.06	2.97	0.80	3.61	1.18	1.19	2.54	2.61	1.34
2	2.58	-	2.56	2.63	2.59	2.48	2.47	2.52	0.93	-	0.77	1.10	1.18	1.16	1.06	1.15
3	2.59	2.83	x	2.85	2.94	2.47	2.42	2.79	1.48	1.74	x	2.89	1.95	4.82	2.40	2.53
4	8.40	-	8.16	8.23	8.25	8.31	8.27	8.40	1.45	-	1.56	2.68	2.77	0.92	1.81	2.07
5	11.4	-	11.3	11.5	11.4	11.4	11.3	11.5	0.83	-	0.83	0.87	0.90	0.88	1.11	1.00
6	14.8	15.0	14.7	14.9	14.9	14.8	14.7	14.9	0.84	0.56	0.75	0.98	1.03	0.83	0.54	0.89
7	15.3	-	15.0	15.6	14.9	14.6	14.4	14.7	2.07	-	1.48	2.53	1.40	1.18	1.37	1.15
8	17.1	-	x	17.2	x	x	x	x	1.22	-	x	0.69	x	x	x	x

Forward Lifting Lug Excitation

	Frequency, Hz								Damping, %							
	0 deg				45 deg	90 deg			0 deg				45 deg	90 deg		
Mode No	Random Shake	Random – low amp	Swept Sine	Impact	Impact	Random Shake	Swept Sine	Impact	Random Shake	Random – low amp	Swept Sine	Impact	Impact	Random Shake	Swept Sine	Impact
1	1.98	-	1.99	2.04	2.06	2.04	2.01	2.08	4.10	-	2.93	1.28	1.10	0.83	2.03	1.13
2	-	-	-	2.61	2.59	-	-	2.54	-	-	-	1.15	1.16	-	-	1.14
3	x	-	x	2.73	3.03	x	2.64	2.89	x	-	x	1.65	2.02	x	1.70	2.17
4	8.35	-	8.23	8.33	8.30	8.44	8.31	8.47	1.31	-	0.98	1.99	2.21	1.30	1.62	1.88
5	11.5	-	11.4	11.6	11.5	11.5	11.4	11.5	0.81	-	0.74	0.76	0.83	0.91	0.92	1.21
6	14.9	-	14.8	15.0	15.0	14.9	14.8	15.0	0.69	-	0.95	0.60	0.56	0.75	0.82	0.63
7	15.5	-	15.5	15.7	14.9	14.7	15.4	14.8	1.48	-	1.41	1.52	1.62	1.31	2.18	1.24
8	x	-	17.0	17.1	x	x	x	x	x	-	0.84	0.85	x	x	x	x

Aft Lifting Lug Excitation

	Frequency, Hz								Damping, %							
	0 deg				45 deg	90 deg			0 deg				45 deg	90 deg		
Mode No	Random Shake	Random – low amp	Swept Sine	Impact	Impact	Random Shake	Swept Sine	Impact	Random Shake	Random – low amp	Swept Sine	Impact	Impact	Random Shake	Swept Sine	Impact
1	2.01	-	2.00	2.04	2.08	2.03	2.03	2.09	1.17	-	2.56	1.30	1.44	1.06	1.16	1.21
2	-	-	-	2.61	2.58	-	-	2.53	-	-	-	1.11	1.10	-	-	1.11
3	2.58	-	x	2.78	3.00	2.71	2.49	2.88	1.12	-	x	2.07	2.01	3.08	1.24	2.29
4	-	-	-	8.32	8.30	-	-	8.47	-	-	-	2.26	2.23	-	-	1.94
5	-	-	-	11.6	11.5	-	-	11.6	-	-	-	0.87	0.85	-	-	1.15
6	15.0	-	14.9	15.0	15.0	15.0	14.9	15.0	0.65	-	0.86	0.61	0.56	0.60	0.92	0.55
7	-	-	-	15.8	14.8	-	-	14.7	-	-	-	1.40	1.62	-	-	1.33
8	-	-	-	17.1	x	-	-	x	-	-	-	0.56	x	-	-	x

- Mode not expected, due to limited shake directions

x Mode expected, but not found or unable to fit